BeBeC-2020-D13

FURTHER DEVELOPMENT OF THE ROSI BEAMFORMING METHOD FOR THE INVESTIGATION OF TURBOMACHINERY INVESTIGATED AT AN ANGLE

Haitian Zhang, Bálint Kocsis, and Csaba Horváth
Budapest University of Technology and Economics, Faculty of Mechanical Engineering, Department of Fluid Mechanics
Bertalan Lajos street 4-6, 1111, Budapest, Hungary

ABSTRACT

The ROtating Source Identifier (ROSI) beamforming algorithm is a method designed for localizing rotating noise sources in a uniform flow utilizing out-of-flow measurements of the acoustic pressure field. It has been developed for sources moving along a circular path, such as turbomachinery blades. The original ROSI method takes the average of the measured acoustic signal over a long time segment in order to reconstruct the noise sources. By doing so, it does not take into consideration certain features of the noise sources, such as differences between the trailing edge and the leading edge noise sources of the given blades. A further development of the method is presented herein, which separates the pressure signal of one revolution of a given noise source into multiple segments. This method will be referred to as the segmented ROSI method. Using this method, the beamforming maps can provide a better understanding as to the differences between the noise sources as a function of angular position. The goal of this further development is to improve the capability of the method in identifying the position-dependent differences between the noise sources that are rotating around an axis. The new segmented ROSI method is presented through a series of example cases, comparing it to the original ROSI algorithm. Though the publication only presents the theory behind the method under development and a few basic validation cases, the results are promising regarding the applicability of the method to other more complex tasks upon fine tuning the method and the associated code.

1 INTRODUCTION

Since their introduction by Billingsley in the 1970s [1], microphone arrays have become the standard equipment for localizing sound sources. Processing the recorded signals using beamforming, phased array microphone systems can be used for localizing noise sources in a wide range of circumstances, such as a moving car, a flying airplane, or a turbine rotor [2]. Though the development of microphone and data storage technology has played a significant role in the fast paced advancement of phased array microphone technology, a proper

beamforming algorithm is essential for a successful noise source localization. The state of the art in the field of acoustic beamforming is therefore continuously improving, with new methods appearing in the literature at a very quick pace. These beamforming methods all offer some advantage over other methods available in the literature, be that a better means of processing a given subset of noise source localization problems, a more efficient algorithm, or a better resolution.

In principle, beamforming algorithms take an investigation area and divide it into grid points, computing the source amplitudes in each grid point from the recorded microphone signals in order to obtain a source amplitude distribution [3]. The most basic beamforming method is the Delay & Sum algorithm [3], which provides the basis of many advanced beamforming methods. Advanced beamforming methods, such as deconvolution methods, take the results one step further, eliminating the dependence of the results on the microphone array used in the investigation. The DAMAS algorithm can be mentioned as a pioneer among these methods [4]. The CLEAN-SC algorithm has also proven to be effective at reducing sidelobe levels, but with a significantly shorter processing time. The CLEAN-SC algorithm is an adaptation of the CLEAN method, initially used in astronomy [5]. Using deconvolution methods, the results seen on beamforming maps can be improved, providing a better sidelobe ratio and broader bandwidth. Though the algorithms mentioned above are able to provide results which highlight the true noise sources much more clearly than the Delay & Sum method, they make a common assumption, in that the investigated noise sources are motionless. However, when the sources are moving, the Doppler Effect comes into play. The ROtating Source Identifier (ROSI) method is a beamforming algorithm specifically designed to overcome the Doppler Effect in the case of rotating sources. The recorded signal goes through a de-Dopplerization step, which shifts the rotating sources back to their reference positions for each timestep. The de-Dopplerized source signals are then processed using a method which corresponds to the Delay & Sum method.

The ROSI algorithm is a very useful tool, e.g. in the case of wind turbines, since the source maps provided by the ROSI algorithm can reveal the areas on the rotor blades, which play a dominant role in the noise generation [6]. Using beamforming methods which do not correct for the source movement (assuming stationary sources) results in beamforming maps having large smeared noise sources, which are spread out along the circumference of the turbomachinery under investigation. However, the original ROSI method has some drawbacks. First of all, the method is formulated in the time domain, which means that it is computationally less efficient than other methods which are formulated in the frequency domain, such as those published in [7] and [8]. Second of all, this means that most advanced beamforming methods cannot be applied in conjunction with the original ROSI method during the processing of the data, which would be possible in the frequency domain (see [7] and [8]). Third of all, when turbomachinery is investigated from a direction which is not axially aligned, but rather from a given viewing angle, different noise sources can be seen, depending on whether the blades are moving toward or away from the observer along their trajectory. These differences provide one with key information regarding the characteristics of the various noise sources, such as the leading edge and trailing edge noise sources. The original ROSI method removes these differences by applying the de-Dopplerization step and then applying a Discrete Fourier Transform on the microphone signals, taking an average over a long time period in reconstructing the source signals. The method does this in order to allow the processing of the signals in the same way that stationary noise source signals would be processed. Information is therefore lost from the source maps. This includes details regarding differences between leading and trailing edge noise sources, as well as airfoil suction and pressure side noise sources. It

should also be mentioned, that if noise sources pass behind a spinner or hub, falling outside of the field of vision of the microphones, false values are averaged into the source maps.

This investigation focuses on the third aspect discussed above, aiming to present the basics of a further development of the original ROSI algorithm, which is capable of identifying the differences between source characteristics as a function of angular position, and will be referred to herein as the segmented ROSI method. The new method presented below therefore divides the captured signal into segments which are shorter than one revolution, enabling one to see the details on the source maps which are not available in the results of the original ROSI algorithm [6] or the frequency domain methods available in the literature [7, 8].

2 CONVENTIONAL BEAMFORMING & ROSI

2.1 Conventional Beamforming

Conventional beamforming using the Delay & Sum method can be described in the following manner. The equations presented here have been described based on [9] and [10]. A microphone array contains N microphones (located at positions $\boldsymbol{x}_n$), and investigates a particular plane, with grid points located at positions $\boldsymbol{x}_m$. An investigated monopole source is located at position $\boldsymbol{x}_s$. In such a case, we can describe the wave propagation by

$$\left\{\frac{1}{c^2}\frac{\partial^2}{\partial t^2} - \Delta\right\} p_n = q_s(t)\delta(\boldsymbol{x}_n - \boldsymbol{x}_s) \tag{1}$$

where p_n is the sound pressure recorded on microphone n, c is the speed of sound, q_s is the source strength, t is the receiver time, and δ is the Dirac-delta function. Under free field conditions, p_n can be obtained by

$$p_n(\boldsymbol{x}_n, t) = \frac{1}{4\pi}\frac{q_s(t-\tau_e)}{|\boldsymbol{x}_n - \boldsymbol{x}_s|} \tag{2}$$

where τ_e is the emission time $\tau_e = |\boldsymbol{x}_n - \boldsymbol{x}_s|/c$.

The Delay & Sum algorithm looks for noise sources at various grid points of the investigation plane by steering the microphone array to each grid point. For each grid point, the reconstructed acoustic source signal σ is therefore attained by propagating the measured sound pressure from each microphone back to each investigated grid point.

$$\sigma_m(\boldsymbol{x}_m, t) = \frac{1}{N}\sum_{n=1}^{N} 4\pi|\boldsymbol{x}_n - \boldsymbol{x}_m| p_{nm}(\boldsymbol{x}_n, t + \tau_{em}) \tag{3}$$

where $\tau_{em} = |\boldsymbol{x}_n - \boldsymbol{x}_m|/c$.

When conducting measurements, microphone signals are sampled, and therefore a discretized signal having a sampling frequency f_s is available for processing. Applying a Discrete Fourier Transform to the signal, the frequency-domain expression of the reconstructed acoustic source signal can be given as

$$\hat{\sigma}_m(\boldsymbol{x}_m, \omega) = \frac{1}{N}\sum_{n=1}^{N} 4\pi|\boldsymbol{x}_n - \boldsymbol{x}_m| \hat{p}_{nm}(\boldsymbol{x}_n, \omega) e^{i\tau_{em}\omega} \tag{4}$$

where i denotes the imaginary unit, $\widehat{(.)}$ is used to show that the value is now in the frequency domain, and ω is the angular frequency. Therefore, the sound source at grid point m is the average of N microphone results.
This equation can be written in vector matrix form by using the stearing vector $\boldsymbol{e}$, which is a column vector, and has components of the form $e^{i\tau_{em}\omega}$, the weighting matrix $\boldsymbol{W}$, which has diagonal components having the form $4\pi|\boldsymbol{x}_n - \boldsymbol{x}_m|/N$ and the column vector of the pressure values $\boldsymbol{P}$, which has components having the form $\hat{p}_n(\boldsymbol{x}_n, \omega)$ as

$$\hat{\sigma}_m(\boldsymbol{x}_m, \omega) = \boldsymbol{e}^{\mathcal{H}}\boldsymbol{W}\boldsymbol{P} \tag{5}$$

where $(.)^{\mathcal{H}}$ is the conjugate transpose.

In most cases the auto power spectrum $\hat{S}_{\sigma\sigma}(\omega)$ is used to display the reconstructed acoustic source signals in terms of beamforming level, on a dB scale.

$$\hat{S}_{\sigma\sigma}(\omega) = \hat{\sigma}_m^*(\omega)\hat{\sigma}_m(\omega) = \boldsymbol{e}^{\mathcal{H}}\boldsymbol{W}\boldsymbol{C}\boldsymbol{W}^{\boldsymbol{\mathcal{H}}}\boldsymbol{e} \tag{6}$$

Where $\boldsymbol{C}$ is the cross-spectral density matrix of the pressure signals. In the in-house software used in this investigation, the pressure signals are sampled into K subsegments and multiplied by a window function in order to reduce the sidelobe effect. $\mathbb{W}$ denotes the normalized window coefficient, and $p_{k,n}^*$ represents the complex conjugate of the kth subsegment of the pressure signal from microphone n.

$$\boldsymbol{C} = \frac{1}{K\mathbb{W}}\begin{bmatrix} \sum_{k=1}^{K}\hat{p}_{k,1}^*\hat{p}_{k,1} & \sum_{k=1}^{K}\hat{p}_{k,1}^*\hat{p}_{k,2} & \cdots & \sum_{k=1}^{K}\hat{p}_{k,1}^*\hat{p}_{k,N} \\ \sum_{k=1}^{K}\hat{p}_{k,2}^*\hat{p}_{k,1} & \sum_{k=1}^{K}\hat{p}_{k,2}^*\hat{p}_{k,2} & \cdots & \sum_{k=1}^{K}\hat{p}_{k,2}^*\hat{p}_{k,N} \\ \vdots & \vdots & \ddots & \vdots \\ \sum_{k=1}^{K}\hat{p}_{k,N}^*\hat{p}_{k,1} & \sum_{k=1}^{K}\hat{p}_{k,2}^*\hat{p}_{k,N} & \cdots & \sum_{k=1}^{K}\hat{p}_{k,N}^*\hat{p}_{k,N} \end{bmatrix} \tag{7}$$

In this way, the beamforming level is computed for each grid point, and the results of the individual grid points can be presented together on a beamforming map that displays the beamforming level distribution in the investigated plane. I.e., the source location is identified.

2.2 ROSI

The ROSI method developed by Sijtsma et al. [6] is specifically designed for sources moving at subsonic speeds. The major innovation of this algorithm is the transfer function, which is applied prior to reconstructing the source distribution, which is referred to as the de-Dopplerization step. This process shifts the rotating sources back to their reference positions and eliminates the temporal changes in the measured sound field which are resulting from the Doppler Effect.

Demonstrating the capabilities of the ROSI method, Oerlemans et al. have conducted measurements on a wind turbine [11]. The results obtained by conventional beamforming and the original ROSI method have been compared in the paper. The conventional beamforming

method results in an extended source area which is smeared along the circumference of the turbomachinery under investigation. This method can only provide a very rough estimate of the source locations. Using the original ROSI algorithm, the results can be resolved in greater detail. The original ROSI method is capable of capturing the results in one reference position for the entire recorded time signal by applying the de-Dopplerization step. The noise sources are then treated as stationary noise sources while carrying out the remaining steps of the beamforming process, which correspond to the steps of the Delay & Sum beamforming method described above. The original ROSI method is therefore able to localize the noise sources to given areas on a rotor.

The ROSI method can be applied on a similar test set up as the Delay & Sum method, for a microphone array having N microphones (located at positions $\boldsymbol{x}_n$), used to investigate a particular plane having grid points located at positions $\boldsymbol{x}_m$. For a moving source located at position $\boldsymbol{x}_s$, at $t = \tau_e$, the wave propagation can be described as

$$\nabla^2 p_n - \frac{1}{c^2}\left(\frac{\partial}{\partial t} + \boldsymbol{U}\nabla\right)^2 p_n = q_s(t)\delta\big(\boldsymbol{x}_n - \boldsymbol{x}_s(t)\big) \tag{8}$$

where $\boldsymbol{U}$ is the uniform flow speed. In [12], the solution of Eq. (8) is derived to be

$$p_{ns}(\boldsymbol{x}_n, t) = \frac{-q_s(\tau_e)}{4\pi\{c(t-\tau_e) + Q(\boldsymbol{x}_n, \boldsymbol{x}_s, t, \tau_e)\}} \tag{9}$$

where $\tau_e = |\boldsymbol{x}_n - \boldsymbol{x}_s(t)|/c$ is the emission time from the moving source to the given microphone of the microphone array and Q is a function of $\boldsymbol{x}_n, \boldsymbol{x}_s, t, \tau_e$, and can be written as

$$Q(\boldsymbol{x}_n, \boldsymbol{x}_s, t, \tau_e) = \frac{1}{c}(-\boldsymbol{x}_s'(\tau_e) + \boldsymbol{U})\big(\boldsymbol{x}_n - \boldsymbol{x}_s(\tau_e) - \boldsymbol{U}(t-\tau_e)\big) \tag{10}$$

The relationship between the recorded pressure and reconstructed acoustic source signal can therefore be given for a moving source

$$\sigma_{nm} = 4\pi[c(t-\tau_{em}) + Q(\boldsymbol{x}_n, \boldsymbol{x}_m, t, \tau_{em})]p_{nm} \tag{11}$$

where $\tau_{em} = |\boldsymbol{x}_n - \boldsymbol{x}_m|/c$.
Taking an average of the reconstructed source signals and carrying out the steps given by Eqs. 4-7, the beamforming source maps can be obtained similarly to what was presented in Chapter 2.1.

3 SEGMENTED ROSI METHOD

3.1 Description of the method

In order to overcome the shortcomings of the original ROSI method described in the introduction, it has been further developed and the new segmented ROSI method is introduced in this section. In a first step, the de-Dopplerization step is carried out, similarly to the original ROSI method. The new method then differs from the original ROSI method in that it separates the de-Dopplerized time domain signals within one revolution into smaller segments as a function of blade position. The size of these segments is user defined, and in this study will be one half a revolution. Following this step, the Discrete Fourier Transform is carried out and the cross-spectral density matrix of the pressure signals is calculated. The cross-spectral density

matrix used in the new segmented ROSI method differs from that used in the original ROSI method, as it is calculated separately for each segment.

If the total recording time interval is T, the source rotates with a rotational frequency f_r, the sampling rate of the microphones is f_s, and the number of segments that are investigated within one revolution is g, then the total number of acoustic pressure data values L collected with microphone n is

$$L = Tf_s \tag{12}$$

The number of samples collected over one segment L_{seg} is

$$L_{seg} = \frac{f_s}{gf_r} \tag{13}$$

The total number of segments N_{seg} is $N_{seg} = L/L_{seg}$, with $n_{seg} = 1, 2, \dots, N_{seg}$. Separating the samples within one segment into K subsegments of window length L_w and with overlap O

$$K = \frac{L_{seg}}{L_w(1-O)} \tag{14}$$

The recorded sound pressure that is assigned to a given segment $p_{n_{seg},k,n}$ is assigned from the recorded sound pressure p_{nm} according to

$$\sigma_{n_{seg},k,n}\left(\frac{l}{f_s}\right) = \sigma_{nm}\left(\frac{l + kL_w(1-O) + n_{seg}L_{seg}}{f_s}\right) \tag{15}$$

where $l = 0, 1, 2, \dots, L_w - 1$ and $k = 0, 1, \dots, K-1$. Next, the Discrete Fourier transform is performed to obtain $\hat{\sigma}_{n_{seg},k,n}(\omega)$. Similarly to Eq. (6), the auto power spectra $\hat{S}_{\sigma\sigma,g}(\omega)$ are calculated with respect to the segments. $N_r = L/f_r$ is the total number of revolutions, $n_r = 0, 1, \dots, N_r - 1$.

$$\hat{S}_{\sigma\sigma,1}(\omega) = \frac{1}{N_r KW}\begin{pmatrix} \sum_{n_r=0}^{N_r}\sum_{k=1}^{K}\hat{\sigma}^*_{gn_r+1,k,1}\hat{\sigma}_{gn_r+1,k,1} & \cdots & \sum_{n_r=0}^{N_r}\sum_{k=1}^{K}\hat{\sigma}^*_{gn_r+1,k,1}\hat{\sigma}_{gn_r+1,k,N} \\ \vdots & \ddots & \vdots \\ \sum_{n_r=0}^{N_r}\sum_{k=1}^{K}\hat{\sigma}^*_{gn_r+1,k,N}\hat{\sigma}_{gn_r+1,k,1} & \cdots & \sum_{n_r=0}^{N_r}\sum_{k=1}^{K}\hat{\sigma}^*_{gn_r+1,k,N}\hat{\sigma}_{gn_r+1,k,N} \end{pmatrix} \tag{16}$$

$$\hat{S}_{\sigma\sigma,2}(\omega) = \frac{1}{N_r KW}\begin{pmatrix} \sum_{n_r=0}^{N_r}\sum_{k=1}^{K}\hat{\sigma}^*_{gn_r+2,k,1}\hat{\sigma}_{gn_r+1,k,1} & \cdots & \sum_{n_r=0}^{N_r}\sum_{k=1}^{K}\hat{\sigma}^*_{gn_r+2,k,1}\hat{\sigma}_{gn_r+1,k,N} \\ \vdots & \ddots & \vdots \\ \sum_{n_r=0}^{N_r}\sum_{k=1}^{K}\hat{\sigma}^*_{gn_r+2,k,N}\hat{\sigma}_{gn_r+1,k,1} & \cdots & \sum_{n_r=0}^{N_r}\sum_{k=1}^{K}\hat{\sigma}^*_{gn_r+2,k,N}\hat{\sigma}_{gn_r+1,k,N} \end{pmatrix} \tag{17}$$

$$\vdots$$

$$\hat{S}_{\sigma\sigma,g}(\omega) = \frac{1}{N_r K W} \begin{pmatrix} \sum_{n_r=0}^{N_r} \sum_{k=1}^{K} \hat{\sigma}^*_{gn_r+g,k,1} \hat{\sigma}_{gn_r+1,k,1} & \cdots & \sum_{n_r=0}^{N_r} \sum_{k=1}^{K} \hat{\sigma}^*_{gn_r+g,k,1} \hat{\sigma}_{gn_r+1,k,N} \\ \vdots & \ddots & \vdots \\ \sum_{n_r=0}^{N_r} \sum_{k=1}^{K} \hat{\sigma}^*_{gn_r+g,k,N} \hat{\sigma}_{gn_r+1,k,1} & \cdots & \sum_{n_r=0}^{N_r} \sum_{k=1}^{K} \hat{\sigma}^*_{gn_r+g,k,N} \hat{\sigma}_{gn_r+1,k,N} \end{pmatrix} \quad (18)$$

The beamforming results can now be presented on multiple beamforming maps as a function of source position, having one beamforming map for each segment of a revolution for every frequency bin under investigation.

3.2 Code Implementation

Based on the new method presented in Chapter 3.1, the segmented ROSI method has been implemented in an in-house beamforming code. The principle steps of the code are presented in Fig. 1. together with the original ROSI method and a second method for segmenting the time domain signal data, which is still under development. This paper is based on one method of segmentation, as presented in the middle column, which separates the segmenst after the de-Dopplerisation step. This approach makes it easier to separate the segments based on the real positions of the sources, without a need to account for the time delay resulting from the wave propagation. In a future step, the second approach for obtaining segments (third column), which is to be carried out before the de-Dopplerisation, will be implemented and the methods will be compared.

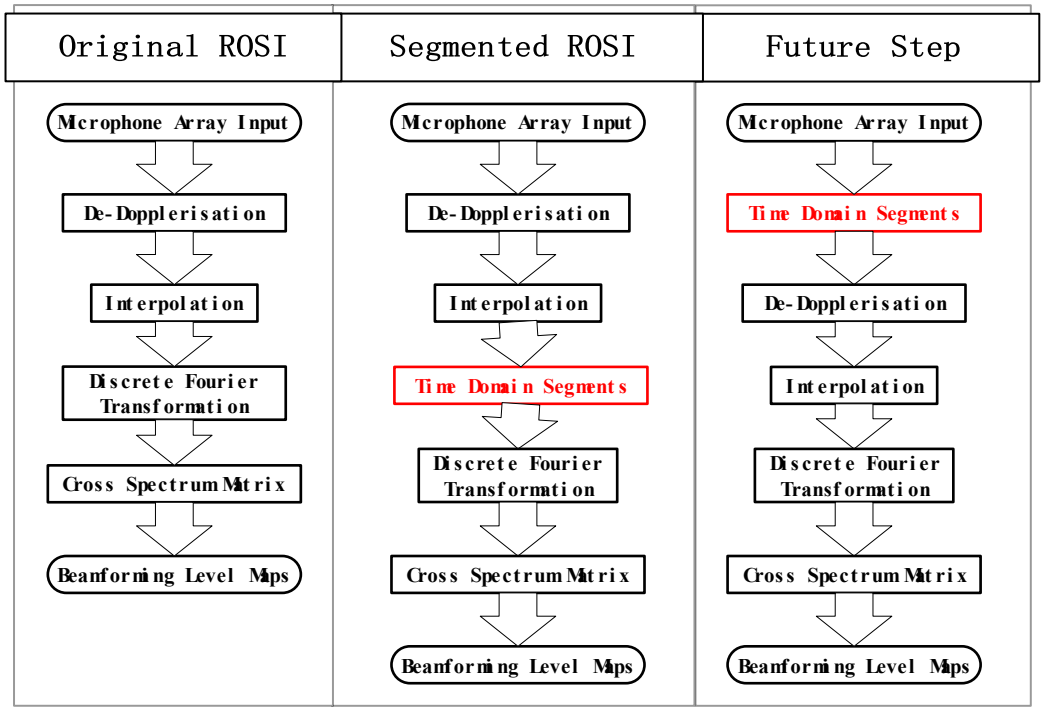

Fig. 1. Flow chart of the new segmented ROSI method

With the current version of the code, the de-Dopplerization with regard to the noise source reference positions is carried out prior to separating the signal into segments. Therefore, even though the signals are segmented after the de-Dopplerization step, the source positions on the beamform maps can still be recognized as being in the reference positions, which, in this case are the initial positions. This approach can both maintain the feature of presenting the reference location of the sound source as in the original ROSI algorithm, as well as highlighting the differences between the noise source characteristics at various angular positions. The advantages of this version are also its disadvantages, as the de-Dopplerization to the same reference position can cause confusion.

4 VALIDATION TEST CASES

The following validation test case simulations have been created in order to demonstrate the capabilities of the segmented ROSI algorithm. The results of the segmented and the original ROSI algorithms are compared below. In each case, one or two monopole noise sources are rotated around the axis in the $z = 0$ plane. The source frequencies of the tonal monopole noise sources are not the same in the case of multiple noise sources within one simulation (3000 Hz and 5000 Hz). The sources can be considered as point sources. Since the test cases have been created numerically, the signal-to-noise ratio is not an issue.

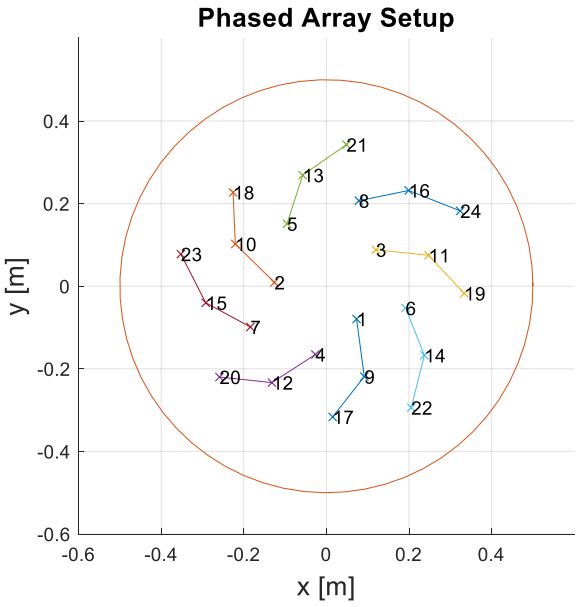

Figure 2 Layout of the virtual phased array

Table 1. Test case settings

	Source number	Source frequency [Hz]	Angular frequency [Hz]	Phased array angle [°]	Distance [m]
Case 1	1	5000	50	-45	1.4
Case 2	2	3000, 5000	50	-45	1.4

The parameters of the test cases are shown in Table 1. The layout of the microphone array is shown in Fig. 2, and the rotor of Case 1 together with the array placement is shown in Fig. 3. The paths along which the noise sources move, their reference positions (initial positions), as well as the microphone positions can be seen on Fig. 3 and Fig. 6 for the two configurations. The virtual microphone array used in the investigation consists of 24 microphones arranged in a spiral pattern. The distance between the center of the array and the center point of the plane of motion of the noise sources is 1.4 m. In Table 1, the phased array angle refers to the angle between the normal direction of the plane of rotation and the normal direction of the array. The negative value refers to counter-clockwise rotation. The angular frequency of the sources is 50 Hz.

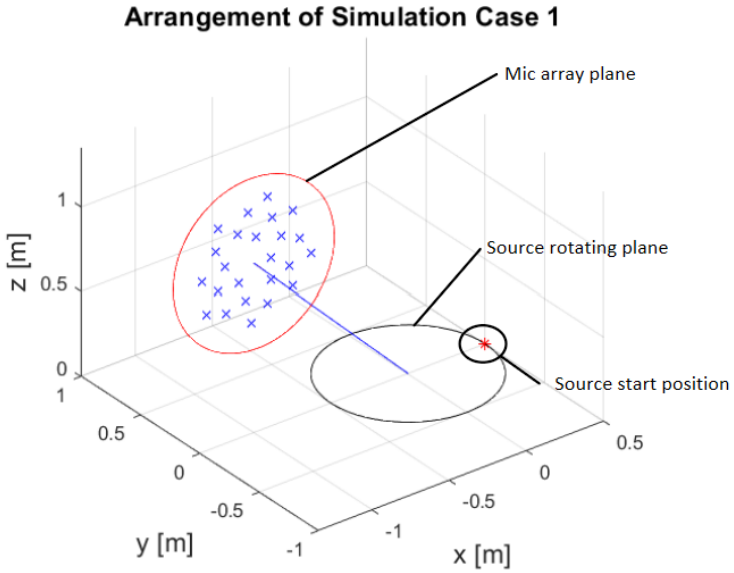

Fig. 3. The arrangement of simulation Case 1.

In each simulation, data was sampled over 50 revolutions. Care was taken to guarantee that the signals from the sources reach all the microphones prior to sampling and storing the data for processing. The sampling frequency used in collecting the data is 512000 Hz. Therefore, the number of samples for each segment is 5120. One might question whether the number of samples used in a real test case will be sufficient for processing data. This will be tested on measurement data in the near future, but it is expected that the possibility for averaging a large amount of data will help in highlighting the true noise sources on the beamforming maps as compared to the sidelobes. With regard to broadband noise sources, it is possible to process more than a single segment worth of data since a window function is used. This will provide an opportunity for processing sample lengths that are longer than one single segment worth of data, decreasing the bandwidth, as well as making it possible to increase the number of segments into which one rotation can be split without information loss.

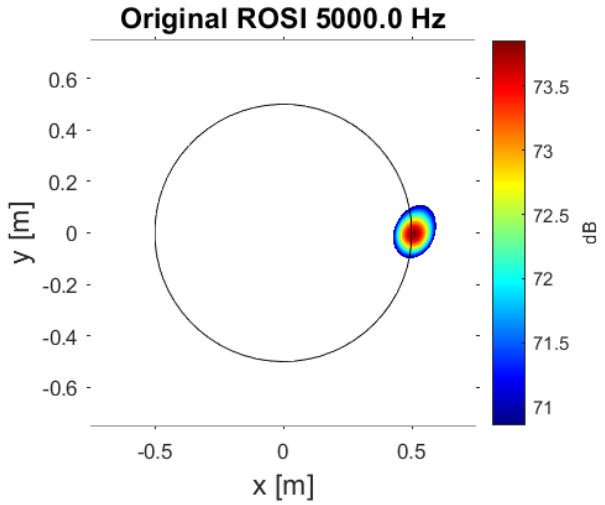

Fig. 4. The results obtained using the original ROSI algorithm for Case 1. The frequency of the sound emitted by the source is 5000Hz.

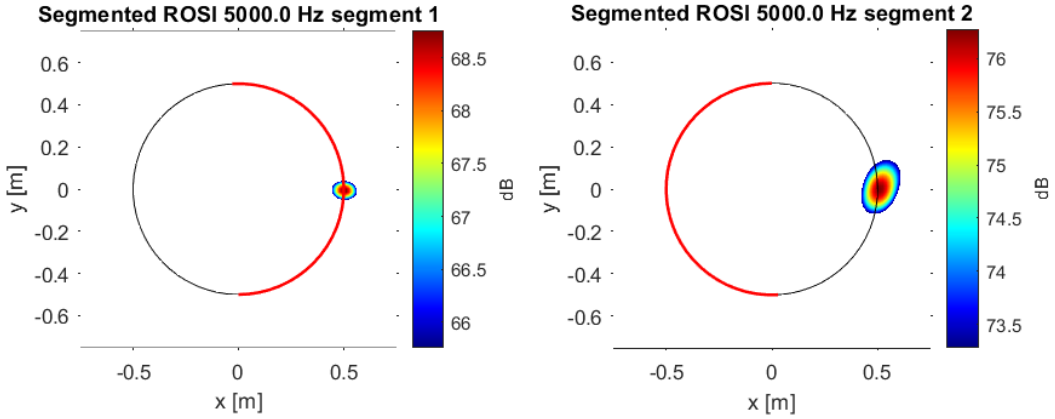

Fig. 5. The results obtained using the segmented ROSI algorithm for Case 1. The frequency of the sound emitted by the source is 5000Hz. The left- and right hand beamforming maps show the results of the two segments. The noise source paths of the segments under investigation are marked in red.

The first test case (Case 1) is used in order to show that the characteristics of a single noise source can be reconstructed along two separate segments by the beamforming method. Case 1 is depicted in Fig. 3. It can be seen that a single noise source moves along a circular trajectory in the plane of rotation. In Fig. 4, the results are as would be expected for a single tonal noise source processed using the original ROSI algorithm. The noise source is localized to its reference position, which in this case coincides with the initial position. The beamforming peak level of the source is near 74 dB. Being a numerical case for a single tonal monopole noise source with a good signal-to-noise ratio, the amplitude of the reconstructed noise source agrees quite well with the amplitude set in the simulation. The results in Fig. 5 present the beamforming maps for the segmented ROSI method for a case where two segments are used. In both cases (both segments), the source is depicted in its reference position, the initial position. Red curves mark the segments for which the given beamform maps are created. As seen on Fig. 3, the phased array is located in the negative x direction. The noise sources are therefore closer to the the noise source when processed on the segment for which x is less than 0. The results

differ from what would be expected, in that the amplitude of the noise source localized along the segment which is physically closer to the array is larger. In theory, it would be expected that the two segments would have very similar noise source maps for a single rotating monopole noise source. This shows that the development of this method is still an ongoing process, and there are details which still need to be fine tuned, but the core concept which is being tested, in other words, the capability of the segmented ROSI method to localize a single rotating monopole noise source along multiple segments has been successfully demonstrated.

In the second test case, two incoherent rotating tonal monopole noise sources are investigated. The arrangement of the simulation for Case 2 is similar to that used in Case 1, with the exception that a second source is added. The arrangement can be seen on Fig. 6. In this case, two rotating monopole noise sources having frequencies of 3000 Hz and 5000 Hz, respectively, are investigated. The length of the investigated segments is one half of a rotation, and therefore each segment will contain only one noise source at a time. The goal of this investigation is to show that the method is capable of processing multiple noise sources. Two noise sources is still a very basic test case, but is the next step in further developing the code and fine tuning its capabilities.

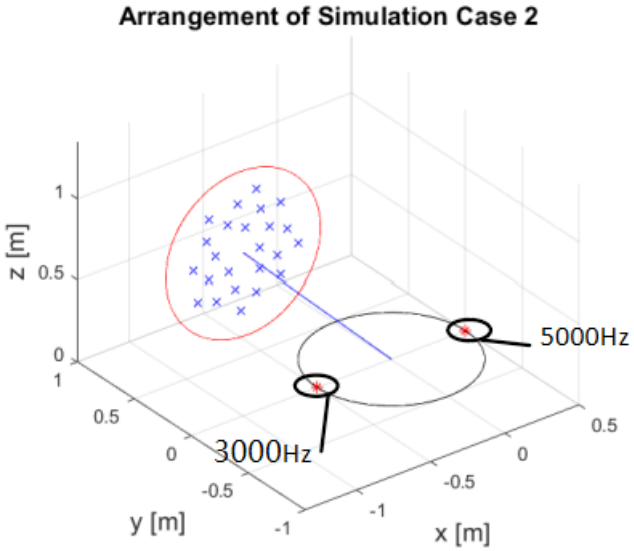

Fig. 6. The simulational arrangement of Case 2.

The results of the original ROSI method, shown on Fig. 7, localize the noise sources to their reference positions, as would be expected. The left side of the figure shows the noise source having a frequency of 3000 Hz, while the right side shows the noise source having a frequency of 5000 Hz. The amplitudes of the noise sources are once again quite close to the amplitude which was set in the simulations. It can be noticed that the noise source which has its reference position in the negative x direction, has once again resulted in a larger size. On the one hand, a noise source of lower frequency would be expected to have a larger size on the beamforming maps. In this case it is not clear whether the results are influenced by the topic discussed in Case 1 above and therefore needs to be further investigated. Comparing the original ROSI and segmented ROSI results for 3000 Hz (Fig. 8), it can be seen that the shape of the noise source for the segment which is on the negative x portion of the trajectory is very similar to the one

acquired with the original ROSI method. The amplitude on the other hand is larger, while it is once again smaller for the positive x portion of the trajectory.

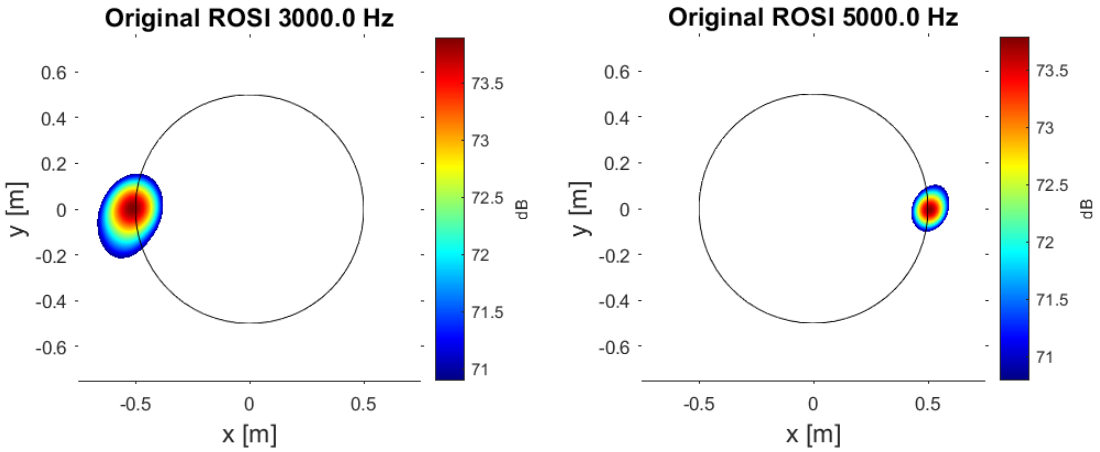

Fig. 7. The obtained results using the original ROSI algorithm in Case 2. The frequencies of the sound emitted by the two sources were 3000 Hz (left) and 5000Hz (right).

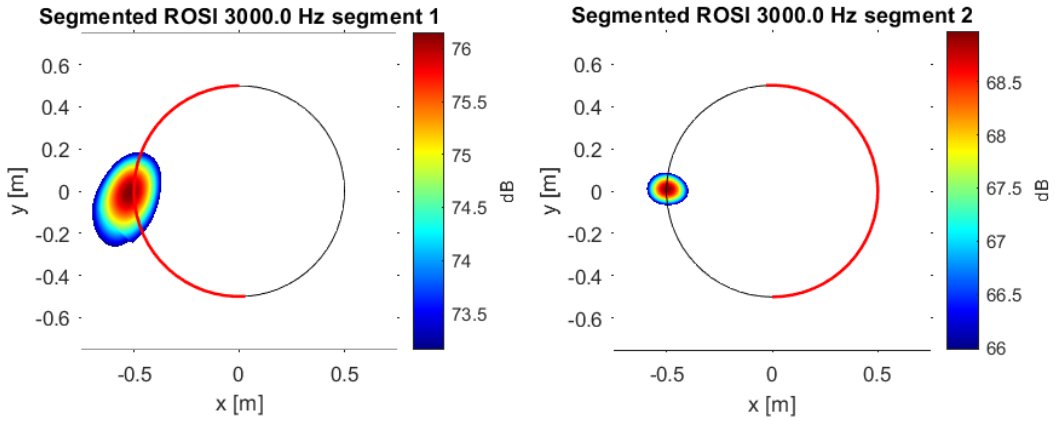

Fig. 8. The obtained results using the segmented ROSI algorithm in Case 2. The frequency of the sound emitted by the source presented here was 3000 Hz. The left- and right sides of the image show the results of the two segments, marked in red.

For the case of the 5000 Hz noise source investigated using the segmented ROSI method (Fig. 9), the same phenomena can be noticed. The size and shape of the noise source received using the segmented ROSI method agrees quite well with the noise source received using the original ROSI method when the source is traveling along the negative x portion of the trajectory, while the amplitude is too large. For the positive x portion of the trajectory, the amplitude is once again smaller. It is hypothesized that the same phenomena which caused the noise sources in Case 1 to not agree entirely with the original ROSI results is responsible for the results in Case 2 not agreeing entirely with what is expected. In summing up the results for Case 2, it can be seen that the segmented ROSI method is able to localize two incoherent rotating tonal monopole noise sources to their reference positions. As concluded from the results for Case 1, the method and related codes are still being tested and fine tuned, and therefore there are many

aspects which still need to be inspected prior to saying that the method has been sufficiently validated.

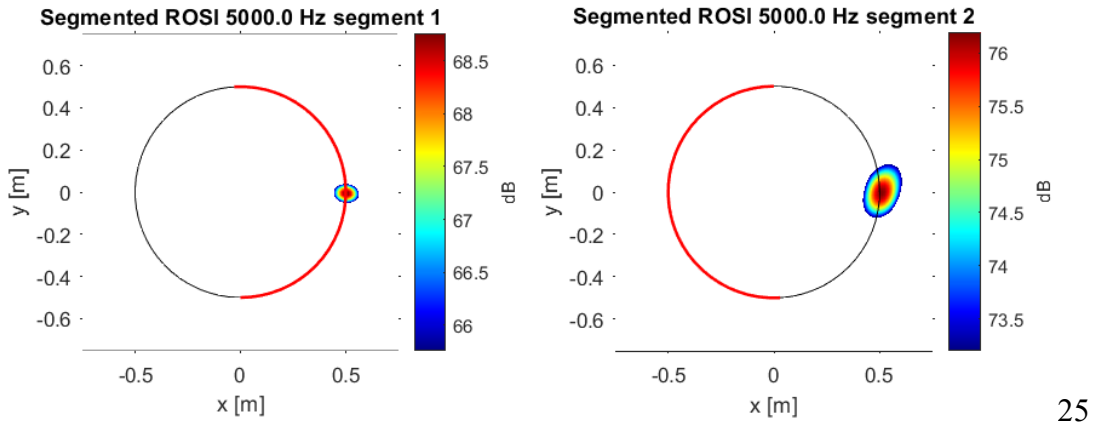

25

Fig. 9. The obtained results using the modified ROSI algorithm in Case 2. The frequency of the sound emitted by the source presented here was 5000 Hz. The left- and right sides of the image show the results of the two segments, marked in red.

5 SUMMARY

The current investigation presents the theoretical background and preliminary results of a novel beamforming method, named segmented ROSI method, which is designed to give a clearer picture regarding those rotating noise sources which only appear along given portions of the trajectory, from the viewpoint of the phased array, such as leading edge, trailing edge, pressure side, and suction side noise sources, appearing on turbomachinery blades. Two means of segmenting the data are introduced in a very basic manner, and compared to the original ROSI method in a flowchart. The difference between the original ROSI method and one means of implementing the segmented ROSI method is described in theory, and two basic test cases are used to show the current capabilities of the implemented segmented ROSI method as compared to the original ROSI method. Though these preliminary results do not agree entirely with what is expected of the method, they encourage us to continue the development, since the results suggest that the method should work sufficiently upon fine tuning the method and the associated code.

In a further step, this method and code will be meticulously examined, in order to determine whether any bugs have remained in them. In parallel, the segmented ROSI method presented in the third column of Fig. 1, but not examined here, will also be implemented and compared to the other two methods. Basic measurements are also being carried out at present in order to validate the method to measurement data, including broadband noise source data, which is expected to experience a significant increase in resolution as a result of the segmented ROSI method. It is expected that the segmented ROSI method will play a key role in many turbomachinery investigations which cannot easily be examined from the axial direction.

6 ACKNOWLEDGEMENTS

This investigation has been supported by the Hungarian National Research, Development and Innovation Centre under contract No. K 129023, and the János Bolyai Research Scholarship

of the Hungarian Academy of Sciences, by the ÚNKP-19-4 New National Excellence Program of the Ministry for Innovation and Technology, by the Higher Education Excellence Program of the Ministry of Human Capacities in the frame of Water science & Disaster Prevention research area of Budapest University of Technology and Economics (BME FIKP-VÍZ), and by the National Research, Development and Innovation Fund (TUDFO/51757/2019-ITM, Thematic Excellence Program).

REFERENCES

[1] J. Billingsley. "An acoustic telescope." Aeronautical Research Council ARC 35/364. 1974.

[2] U. Michel. "History of acoustic beamforming." In: Proceedings of the 1st Berlin Beamforming Conference, Berlin, Germany, 21-22. November 2006.

[3] R.P. Dougherty. "Beamforming in acoustic testing." in Aeroacoustic Measurements, edited by T. J. Mueller, pp. 62–97, Springer, Berlin, 2002.

[4] T. F. Brooks and W. M. A. Humphreys. "Deconvolution approach for the mapping of acoustic sources (DAMAS) determined from phased microphone arrays." AIAA-2004–2954, 2004. 10th AIAA/CEAS Aeroacoustics Conference, Manchester, Great Britain, 10-12 May 2004. doi10.2514/6.2004-2954.

[5] R.P. Dougherty and R.W. Stoker. "Sidelobe suppression for phased array aeroacoustics measurements." AIAA-98-2242, 1998. 4th AIAA/CEAS Aeroacoustics Conference, Toulouse, France, 2-4 June 1998. doi:10.2514/6.1998-2242.

[6] P. Sijtsma, S. Oerlemans and H. Holthusen. "Location of rotating sources by phased array measurements.", AIAA 2001-2167, 2001. 7th AIAA/CEAS Aeroacoustics Conference and Exhibit, Maastricht, Netherlands, 28-30 May 2001. doi:10.2514/6.2001-2167.

[7] G. Herold, and E. Sarradj. "Microphone array method for the characterization of rotating sound sources in axial fans." Noise Control Engineering Journal, Vol. 63, Issue 6, 546-551, 2015.

[8] W. Pannert, and C. Maier. "Rotating beamforming – motion-compensation in the frequency domain and application of high-resolution beamforming algorithms." Journal of Sound and Vibration, Vol. 333, Issue 7, 1899-1912, 2014.

[9] L. Koop. "Beam forming methods in microphone array measurements - Theory, practice and limitations." VKI Experimental Aeroacoustics in collaboration with EWA, Brüssel, Belgium, 13-17 November 2006.

[10] B. Tóth. "Algorithmic Methods for Evaluating Axial Fan Beamforming Maps." PhD thesis, 2019. URL https://repozitorium.omikk.bme.hu/handle/10890/13114.

[11] S. Oerlemans, G. Schepers, G. Guidati and S. Wagner. "Experimental demonstration of wind turbine noise reduction through optimized airfoil shape and trailing-edge serrations." to be presented at the European Wind Energy Conference and Exhibition, Copenhagen, Denmark, 2-6 July 2001.

[12] P. Sijtsma. "Beamforming on moving sources.", VKI Experimental Aeroacoustics in collaboration with EWA, Brüssel, Belgium, 13-17 November 2006.